

Phonon-induced disorder in dynamics of optically pumped metals from non-linear electron-phonon coupling

John Sous,^{1,*} Benedikt Kloss,² Dante M. Kennes,^{3,4} David R. Reichman,^{2,†} and Andrew J. Millis^{1,5,‡}

¹*Department of Physics, Columbia University, New York, New York 10027, USA*

²*Department of Chemistry, Columbia University, New York, New York 10027, USA*

³*Institut für Theorie der Statistischen Physik, RWTH Aachen, 52056 Aachen,*

Germany and JARA - Fundamentals of Future Information Technology

⁴*Max Planck Institute for the Structure and Dynamics of Matter and*

Center for Free-Electron Laser Science, 22761 Hamburg, Germany

⁵*Center for Computational Quantum Physics, Flatiron Institute,*

162 5th Avenue, New York, New York 10010, USA

(Dated: September 3, 2020)

The non-equilibrium dynamics of matter excited by light may produce electronic phases that do not exist in equilibrium, such as laser-induced high- T_c superconductivity. Here we simulate the dynamics of a metal driven at $t = 0$ by a pump that excites dipole-active vibrational modes that couple quadratically to electrons, and study the evolution of its electronic and vibrational observables. We provide evidence for enhancement of local electronic correlations, including double occupancy, accompanied by rapid loss of long-range spatial phase coherence. Concurrently, the onsite vibrational reduced density matrix evolves from its initial coherent state to one with a predominantly diagonal structure whose distribution qualitatively resembles the coherent state Poisson character. This rapid loss of coherence controls the electronic dynamics as the system evolves towards a correlated electron-phonon long-time state. We show that a simple model based on an effective disorder potential generated by the oscillator dephasing dynamics for the electrons provides an explanation for the flattening in momentum of electronic correlations. Our results provide a basis within which to understand correlation dynamics of vibrationally coupled electrons in pump-probe experiments.

I. INTRODUCTION

Major efforts in condensed-matter physics are currently focused on the means to induce novel phases of matter and harness their properties for practical gain. For many years such phases were thought to robustly exist only as equilibrium, thermodynamic states. The potential out-of-equilibrium induction of transient phases, enabled by recent experimental advances in the creation and utilization of tailored time-resolved external fields that can excite specific degrees of freedom, may bypass these limitations [1, 2], opening a door to the realization and control of new electronic states.

Optical, mode-specific excitation of atomic vibrations [3] serves as one broad class of out-of-equilibrium technique that has been shown to lead to dramatic modifications in electronic behavior [4–6], including the possible induction of a superconducting transition at a critical temperature larger than its static counterpart in K_3C_{60} [7], $YBa_2Cu_3O_{6.5}$ [8] and organic salts [9]. In general, since optically accessible phonons are long-wavelength dipole-active modes, these phonons do not couple linearly to electrons, and therefore non-linearities are expected to govern the dynamics in centrosymmetric systems [10–13], stimulating many interesting theoretical proposals [13–20]. One particular mechanism [13] posits

that since direct, local interaction between electrons and photo-excited phonons must depart from that of conventional linear (Holstein [21] and Fröhlich [22, 23]) models, one must consider a quadratic coupling of driven phonons to the electron density (Appendix A). An approximate analysis of such a model suggests that optical driving of quadratically coupled phonons implies a particular form of electronic squeezing of phonons that results in both an effective electron-electron attraction and a random phonon-state-dependent onsite potential for the electrons (Appendix B).

In this work, we use exact numerical methods to explore the emergent electronic behavior in such a driven, non-equilibrium system. Combining a tensor-network approach for time evolution of an infinite one-dimensional system on short timescales with propagation to long times using direct Krylov subspace methods for finite-size systems, we elucidate the spatially resolved dynamics of electrons coupled to pumped phonons. Our main results are:

1. Phonon-induced disorder: We observe fast growth of local electronic correlations after the application of the pump. A dramatic flattening in momentum of charge, spin and pairing correlations rapidly follows, pointing to loss of spatial phase coherence. We study the coherence of the local oscillator and find that its reduced density matrix in the phonon-number basis rapidly relaxes from its initial coherent state [24] to a predominantly diagonal matrix. The diagonal matrix elements/populations in the phonon-number basis form a unimodal distribution very similar to the Poisson distribution that describes the

* js5530@columbia.edu

† drr2103@columbia.edu

‡ ajm2010@columbia.edu

eigenvalues of the coherent state density matrix. Thus, from the perspective of the electrons, the rapid phonon dephasing induces a random onsite potential, which destroys the (quasi-)long-range character of the initially present normal state electronic correlations. This behavior is one of the main predictions of [13].

2. Correlated electron-phonon steady state: We provide evidence that the system evolves to a steady state at long times characterized by sizeable correlations between electrons and phonons. The early-time dynamics that follow the pump already indicate rapid growth of local, negative correlations between the electron density \hat{n} and the oscillator quadratic displacement \hat{X}^2 at a given site and anticorrelations of \hat{X} at adjacent sites, which signals a tendency towards charge flow between neighboring sites, resulting in enhanced double occupancy. This dynamical process quenches the Friedel oscillations [25] of the electron density profile, and manifests as a space-time dependent feature in the density-density correlation function that spreads spatially outwards along a “light-cone” defined by the Fermi velocity [26]. However, behind the light cone, very quickly the density-density correlation function becomes basically structureless, suggesting that the asymptotic state possesses a large degree of randomness. At long times, we find an overall increase in the magnitude of the electron-phonon interaction term, implying evolution towards a strongly correlated long-time electron-phonon state.

3. Quadratically coupled electrons exhibit a greater response to optical pumping than linearly (Holstein) coupled electrons: We compare the dynamical electronic behavior in response to a pump in the quadratic model against that in the linear (Holstein) counterpart. We observe larger double occupancy and greater large-amplitude response of momentum-resolved correlation peaks in the quadratic model. This highlights the importance of the quadratic coupling in irradiated materials.

II. PHYSICAL SETUP

We consider a metal whose vibrational modes are excited at initial time by a light field, e.g., an optical pump. Radiation creates a dipolar coherent phonon field [24] on every site, which couples non-linearly to the local electron density. The Hamiltonian that governs the dynamics is given by

$$\mathcal{H} = \mathcal{H}_e + \mathcal{H}_{\text{ph}} + \mathcal{V}_{\text{e-ph}}. \quad (1)$$

Here $\mathcal{H}_e = -J \sum_{i,\sigma} c_{i,\sigma}^\dagger c_{i+1,\sigma} + \text{H.c.}$ characterizes the dynamics of electrons of spin flavor $\sigma \in \{\uparrow, \downarrow\}$ via the fermion creation (annihilation) operator $c_{i,\sigma}^\dagger$ ($c_{i,\sigma}$) and defines the total charge density $\hat{n}_i = \sum_\sigma \hat{n}_{i,\sigma}$ at site i . The electrons of this irradiated system couple locally to the excited vibrations via the the dominant symmetry-allowed interaction

[13, 27]

$$\mathcal{V}_{\text{e-ph}} = g_q \sum_i (\hat{n}_i - 1)(b_i^\dagger + b_i)^2. \quad (2)$$

The phonon energy-scale is set by $\mathcal{H}_{\text{ph}} = \omega \sum_i \left(b_i^\dagger b_i + \frac{1}{2}\right)$, which characterizes a local optical Einstein phonon mode with frequency ω ($\hbar = 1$), described by the boson creation (annihilation) operator b_i^\dagger (b_i).

We simulate the time evolution of the initial state

$$|\Psi\rangle = |\text{FS}\rangle \otimes \bigotimes_i |\alpha\rangle_i. \quad (3)$$

Here $|\text{FS}\rangle = \prod_{k \leq k_F} c_{k,\sigma}^\dagger |0\rangle$ with $k_F = \pi/2$ describes a metal formed from a Fermi sea of spinful electrons in a half-filled ($\langle \hat{n}_i \rangle = 1$) one-dimensional (1D) lattice and $|\alpha\rangle = e^{-\frac{|\alpha|^2}{2}} \sum_\nu \frac{\alpha^\nu}{\sqrt{\nu!}}$ represents a coherent state of amplitude α written as an appropriate superposition of phonon-number states $|\nu\rangle$. Since the wavelength of the pump field extends beyond the lattice scale, we assume it instigates a perfectly phase-coherent initial product state of onsite phonon coherent states $\bigotimes_i |\alpha\rangle_i$.

This model implies an equilibrium renormalization of the oscillator stiffness $K \rightarrow K[1 + 4\frac{g_q}{\omega}(\langle \hat{n} \rangle_i - 1)]$. The onsite harmonic oscillator is stable so long as $|g_q| < \frac{\omega}{4}$ [13] (Appendix A). We consider here $g_q \leq 0.25$ for $\omega = \pi/2, \pi$ to study dynamics of the non-linear model for couplings ranging from weak to strong. We use $\alpha = \sqrt{2}$ in what follows.

III. METHODS

We simulate the time evolution of $|\Psi\rangle$ representing the metal on an infinite chain irradiated at initial time $t = 0$ by a pump via the infinite time-evolved block decimation (iTEBD) algorithm [28] utilizing the TeNPy Library [29]. We use up to $d_\nu = 12$ phonon states to represent the local phonon Hilbert space. We allow the bond dimension χ to grow without saturation in the iTEBD time evolution, and converge our results with respect to the truncation error ϵ_{TEBD} . This allows access to time $t \sim 5J$ for which we find $\epsilon_{\text{TEBD}} = 10^{-3.5}$ achieves satisfactory convergence. We refer the reader to Appendix C for more information. To shed light on the long-time behavior we also propagate the initial state using direct Krylov subspace methods for finite system sizes $L = 3 - 6$ with twisted boundary conditions, see Appendix D for more details.

IV. RESULTS

Fig. 1 demonstrates the energy redistribution amongst the different system subsectors in the course of the time evolution on timescales ranging from short (left panel) to long (right panel), as the system approaches its long-time limit of a correlated electron-phonon steady state.

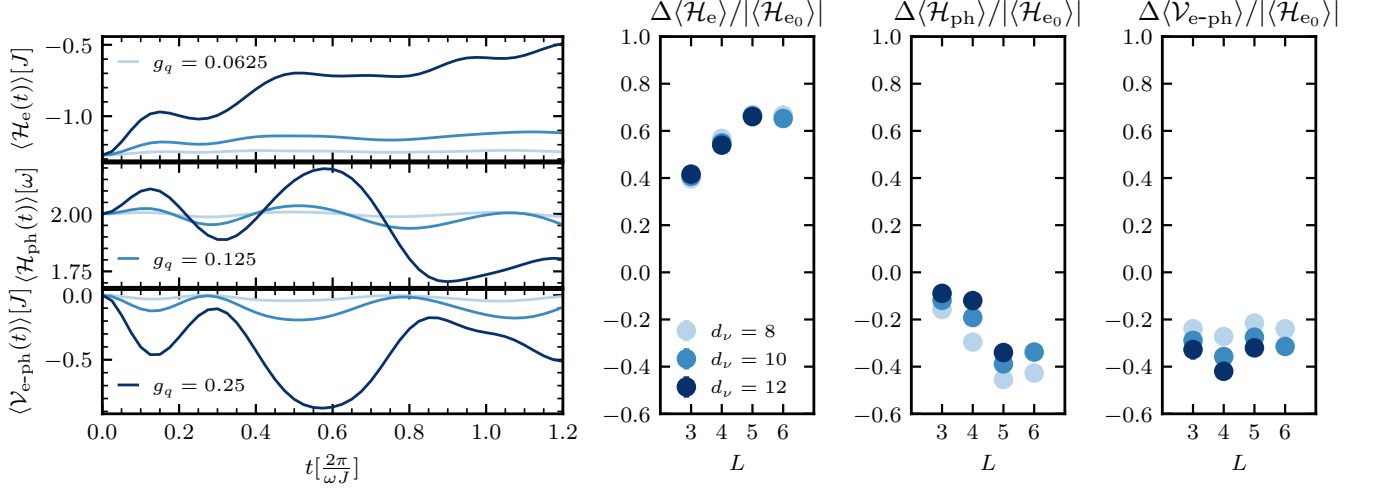


FIG. 1. **Energy redistribution among the different system subsectors.** Infinite system iTEBD simulations (left panel) of the time dependence of the electronic (top), phononic (middle) and electron-phonon (bottom) energy densities show a trend with larger g_q of rapid heating of the electronic subsector, accompanied by transient relaxation of the electron-phonon subsector. Exact Krylov propagation of small systems $L = 3 - 6$ (right panel) for the largest coupling strength $g_q = 0.25$ to asymptotically long times showing the net change relative to the initial state in electronic (left), phononic (center) and electron-phonon (right) energy densities confirms a correlated electron-phonon steady state, as evidenced by the considerable flow of energy from the electron-phonon subsector to the electronic subsector. The y-axis labels of the net change in energy densities have been placed at the top of the corresponding plots. Here $\mathcal{H}_{e_0} \equiv \mathcal{H}_e(0)$.

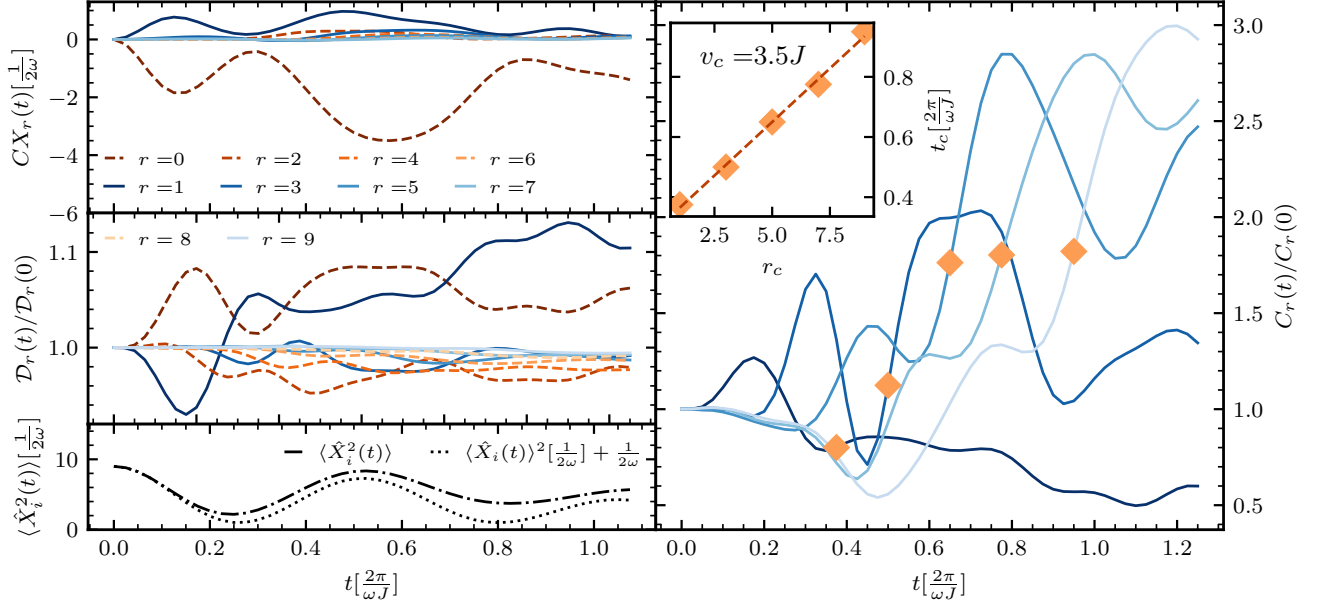


FIG. 2. **Dynamics of charge and charge-phonon correlations.** *Left column:* Time evolution of charge-lattice correlation $CX_r(t) = \langle \hat{n}_i \hat{X}_{i+r}^2(t) \rangle - \langle \hat{n}_i(t) \rangle \langle \hat{X}_{i+r}^2(t) \rangle$ (top) contrasted against that of $\langle \hat{X}_i^2(t) \rangle$ (bottom), and of the (connected) density-density correlation $D_r(t) = \langle \hat{n}_i \hat{n}_{i+r}(t) \rangle$ normalized with respect to its initial-time value $D_r(0)$ (middle). Here $\hat{X}_i := \sqrt{\frac{1}{2M\omega}}(b_i^\dagger + b_i)$, where M is the oscillator mass, which we set to unity, $M = 1$. Note the violation of the relation $(\Delta X_i(t))^2 = \langle \hat{X}_i^2(t) \rangle - \langle \hat{X}_i(t) \rangle^2 = \frac{1}{2\omega}$ for $t \gtrsim 0.15 \frac{2\pi}{\omega J}$, an indication of deviation of the oscillator from an ideal coherent state. *Right column:* Onset of a light-cone profile in the normalized density-density charge correlations; here $C_r(t) = \langle \hat{n}_i \hat{n}_j(t) \rangle - \langle \hat{n}_i(t) \rangle \langle \hat{n}_j(t) \rangle$ is normalized with respect to its initial-time metallic Friedel oscillations profile $C_r(0)$. The diamond symbols mark the inflection point preceding the second maximum for the different r lines, which we use in the inset to find a best fit of the light-cone charge propagation t_c versus r_c (dashed line), yielding an estimate for charge velocity: $v_c \approx 3.5J$. We use $g_q = 0.25$ and $\omega = \pi/2$ in this figure.

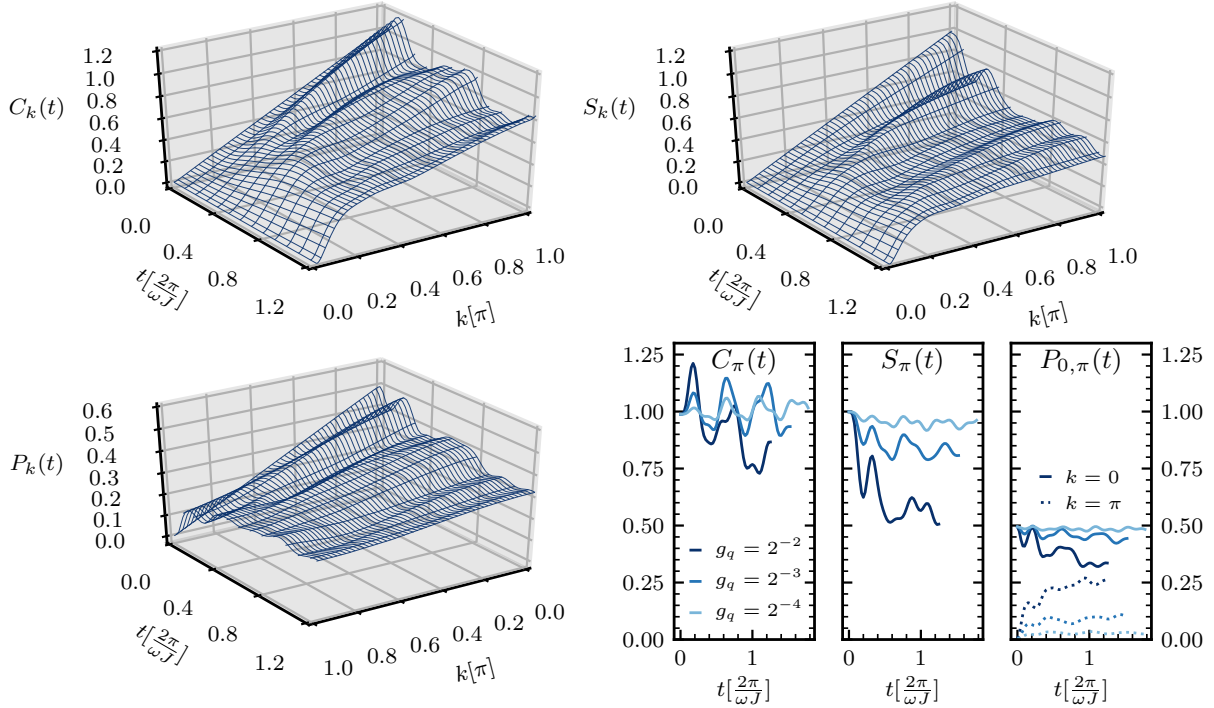


FIG. 3. **Dynamics of momentum-resolved electronic correlations.** We study the evolution with time of momentum-resolved charge $C_k(t) = \mathcal{F}\{C_r(t)\}$, spin $S_k(t) = \mathcal{F}\{S_r(t)\}$ and Pairing $P_k(t) = \mathcal{F}\{P_r(t)\}$ correlation functions for $g_q = 0.25$ and $\omega = \pi/2$ (three-dimensional plots), and the dependence on time of certain k ($0, \pi$) correlations for $\omega = \pi/2$ (bottom, right). Note the k -axis of the $P_k(t)$ plot has been inverted for better visibility, and the y-axis labels of the $0/\pi$ correlations in the bottom right panel have been placed at the top of the corresponding plots. Here $C_r \equiv \langle \hat{n}_i \hat{n}_{i+r} \rangle - \langle \hat{n}_i \rangle \langle \hat{n}_{i+r} \rangle$, $S_r \equiv \langle (\hat{n}_{i,\uparrow} - \hat{n}_{i,\downarrow})(\hat{n}_{i+r,\uparrow} - \hat{n}_{i+r,\downarrow}) \rangle$ and $P_r \equiv \langle c_{i,\uparrow}^\dagger c_{i,\downarrow}^\dagger c_{i+r,\downarrow} c_{i+r,\uparrow} \rangle$. \mathcal{F} denotes the Fourier transform. Charge, spin and pairing correlations all rapidly flatten in the course of the dynamics. Note conservation of $C_0(t)$ and $S_0(t)$ in the dynamics.

Consider the largest coupling $g_q = 0.25$ (dark lines in left panel). At early times $t \leq \frac{2\pi}{\omega J}$, the electron subsystem absorbs energy from the phonons, and the phonon energy density oscillates about a value close to its initial value, while the electron-phonon energy density becomes more negative, see left panel of Fig. 1. At asymptotically long times, we observe an overall flow of energy from the phonon and electron-phonon subsectors to the electron subsector (right panel of Fig. 1). Importantly, the increase in magnitude of the (negative) electron-phonon correlation term implies a long-time correlated electron-phonon state.

Correlations between electrons and phonons already manifest in the early-time dynamics, as we demonstrate in Fig. 2. Consider the charge-phonon correlation function $CX_r(t) = \langle \hat{n}_i \hat{X}_{i+r}^2(t) \rangle - \langle \hat{n}_i(t) \rangle \langle \hat{X}_{i+r}^2(t) \rangle$ (Fig. 2, left; top). For $r = 0$, \hat{n} rapidly becomes negatively correlated with \hat{X}^2 . Note that $\langle \hat{n}_i(t) \rangle = 1$ throughout the dynamics in the translationally invariant system under consideration and $\langle \hat{X}_i^2(t) \rangle$ (dashdotted line, bottom) remains positive under time evolution. The substantial local, neg-

ative correlations in $CX_0(t)$ therefore imply a flow of electrons between neighboring sites. The same analysis applied to $CX_1(t)$ reveals a positive correlation between electron density and phonons separated by a single site with a dynamical profile somewhat similar (albeit of opposite sign) to $CX_0(t)$. With a slightly delayed onset, much weaker positive correlations build up at larger r in $CX_r(t)$. The interplay between onsite and nearest-neighbour correlations in $CX_r(t)$ reflects the tendency of charge to flow from a site to its neighbours, implying that doublons (doubly occupied sites) and holons (empty sites) emerge in the dynamics on such timescales. Indeed, in the middle panel, we observe a rapid enhancement of local electron density-density correlations $\langle \hat{n}_i \hat{n}_i(t) \rangle = \langle \hat{n}_i \rangle + 2\langle \hat{n}_{i,\uparrow} \hat{n}_{i,\downarrow}(t) \rangle$, accompanied by the suppression of $\langle \hat{n}_i \hat{n}_{i+1}(t) \rangle$ due to doublon creation, as expected if there is a tendency towards formation of an alternating pattern of doubly and singly occupied sites. For times greater than $t \approx 0.175 \frac{2\pi}{\omega J}$, $\langle \hat{n}_i \hat{n}_{i+1}(t) \rangle$ begins to grow and becomes positive, whilst $\langle \hat{n}_i \hat{n}_{i+2}(t) \rangle$ diminishes, and a wavefront behavior in r appears to arise. In fact,

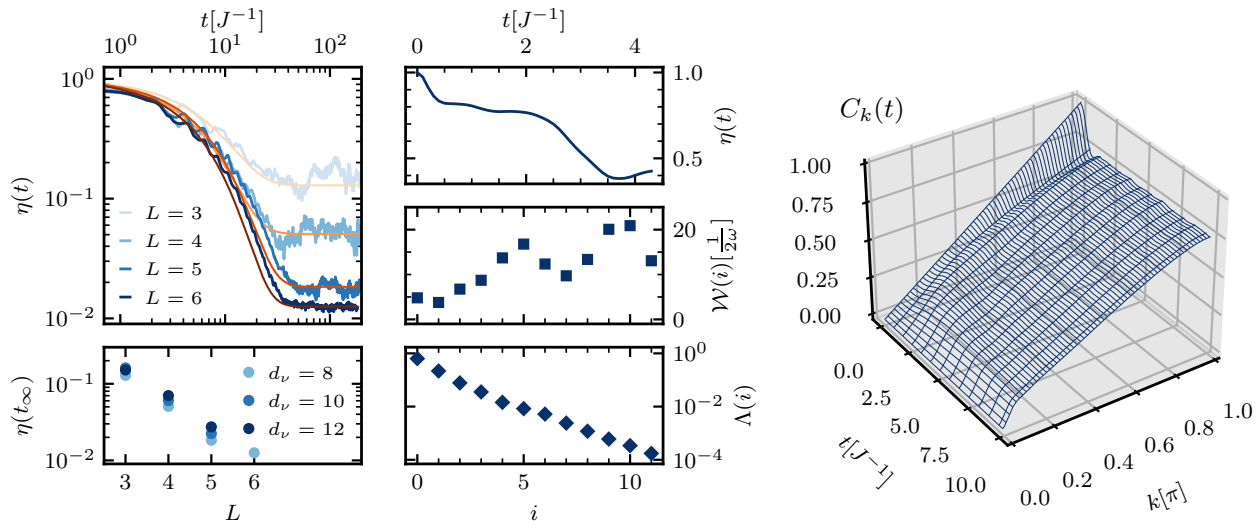


FIG. 4. **Dynamics of a metal subjected to a quadratic coupling, dephasing phonon-generated disorder.** *Left column:* Rapid loss of coherence in the onsite phonon reduced density matrix ρ_{ph}^R shown via analysis of $\eta(t) \equiv \sum_{i \neq j} |\rho_{\text{ph},i,j}^R(t)| / \sum_{i \neq j} |\rho_{\text{ph},i,j}^R(0)|$. This is verified in Krylov propagation of systems of increasing size (left), and can be already observed on short timescales for infinite systems studied by iTEBD (center column, top). Thin lines in orange hues are fits of $\eta(t)$ to an exponential decay to a plateau (top). In the long-time limit, $\eta(t_\infty)$ approaches increasingly vanishing values with larger system sizes (bottom). *Center column:* We use the approach to diagonality of ρ_{ph}^R in iTEBD simulations (top) to invoke a semi-classical approximation in which we treat the phonons classically, as characterized by their reduced density matrix. We extract a disorder potential from the coupled model for an exemplary time $t_q = \frac{2\pi}{\omega J}$ via singular value decomposition of ρ_{ph}^R , which we use to evaluate an effective classical disorder potential $\mathcal{W}(i)$ given by the expectation value of \hat{X}^2 in the singular vectors $i_{S(\rho_{\text{ph}}^R)}$ (middle), and weighed by the probability distribution $\Lambda(i)$ given by the singular values (bottom). *Right column:* We model the dynamics of the electrons quenched to the dephasing phonon potential given by $\mathcal{W}(i)$ weighted by the probability distribution $\Lambda(i)$. A free metal subjected to this disorder potential at initial time exhibits, after disorder averaging, a flattened charge correlator $C_k(t)$ with a suppressed peak, qualitatively supporting the result of the fully coupled model observed in Fig. 3. We use $g_q = 0.25$ and $\omega = \pi/2$ in the simulations of the fully coupled model used in this figure.

when normalized against the $t = 0$ metal Friedel density profile, a density-density correlation light-cone [26, 30] propagating outwards in r can be clearly seen (Fig. 2, right). A characteristic feature that emerges for larger r at later time delays closely trails the second-in-time maximum. Thus, to sharply characterize the light-cone, we track the inflection point preceding that maximum (diamond symbols). A line of best fit through these data points (Fig. 2, right; inset) reveals linear charge propagation with a velocity $v_c \approx 3.5J$, slightly larger than the free metal Fermi velocity $2k_F J = \pi J$. On the timescales accessed by iTEBD, we found no evidence for a wavefront propagating in either of $CX_r(t)$ or $\langle \hat{X}_i(t) \hat{X}_{i+r}(t) \rangle$, reflecting the resistance to propagation of the dispersionless Einstein oscillator modes of the initial-time ($g_q = 0$) state.

The behavior exhibited by $CX_r(t)$ and $C_r(t)$ implies non-equilibrium induction of enhanced double occupancy, which we have directly verified. (For a comparison against the Holstein model, see Fig. 5 and accompanying discussion below).

Turning to Fig. 3, we study the evolution with time of the momentum-resolved charge $C_k(t)$, spin $S_k(t)$ and pairing $P_k(t)$ correlations to fully characterize the elec-

tronic features. Apart from a fast initial growth of $C_\pi(t)$ due to the enhanced double occupancy, we observe rapid flattening in momentum space of these correlations, marking the loss of spatial phase coherence, despite the persistent growth of local density-density and charge-phonon correlations, indicating that the pattern of doubly and singly occupied sites is becoming random. This points to a more subtle role played by phonons in the dynamics, as we explain below.

To understand the nature of these featureless correlations, we analyze the loss of coherence with time of the onsite oscillator reduced density matrix $\rho_{\text{ph}}^R(t)$ in the phonon occupation-number basis. We study the quantity $\eta(t) \equiv \sum_{i \neq j} |\rho_{\text{ph},i,j}^R(t)| / \sum_{i \neq j} |\rho_{\text{ph},i,j}^R(0)|$ as a measure of decoherence (Fig. 4 left, top and center, top panels). We find that $\eta(t)$ drops sharply from its initial value of unity corresponding to the pure initial phonon state to below 50% at $t \sim 4J^{-1}$ and to vanishingly small values in the long-time limit. This implies that $\rho_{\text{ph}}^R(t)$ evolves from its initial pure coherent state $|\alpha\rangle\langle\alpha|$ to a mixed state that is predominantly diagonal in the phonon-number basis, signalling rapid dephasing of states with different phonon occupation number. The dephased configuration exhibits

a unimodal distribution of diagonal matrix elements. Our numerics reveals a strong sensitivity of the electron dynamics to the approach of ρ_{ph}^R to diagonality, as also corroborated in finite-size systems in which we find the phonon coherence and energy densities both relax on the same characteristic timescale $t \sim 5J$. This suggests that the diagonal matrix elements of the \hat{X}^2 operator can be thought of as a slowly evolving classical dynamical onsite potential for the electrons, in other words, as a phonon-generated disorder that destroys long-ranged electronic density wave order, as predicted in Ref. [13].

To verify this picture we compute the dynamics of a metal quenched at initial time to a static, onsite disorder potential extracted from the dephased phonon state, given by $\mathcal{W}(i)$ and weighted by the probability distribution $\Lambda(i)$, where $i \equiv i_{\mathcal{S}(\rho_{\text{ph}}^R)}$ labels the singular vectors of ρ_{ph}^R , see Fig. 4, center column. We find that the momentum-resolved charge dynamics exhibits a rapid flattening over relatively short times (Fig. 4, right column), bolstering the dephasing phonon-induced disorder picture of electron dynamics in the pumped metal. The pump-activated *transient* phonon-induced disorder in electron dynamics presents an opportunity to explore the interplay between correlations and randomness in out-of-equilibrium electronic matter.

Before we conclude, we contrast the dynamics of our non-linear model to that governed by the Holstein model (which, for dipole-active phonons, does not respect inversion symmetry). We use two methods to choose an appropriate coupling strength in the Holstein model corresponding to a given coupling strength of the quadratic model against which we perform a comparison, see Appendix E for details. In one approach we choose the Holstein coupling that yields the same equilibrium ground state double occupancy as in the quadratic model. In the other the Holstein coupling is chosen to produce the same double occupancy as that obtained analytically from a disentangling transformation [13] derived as a low-energy description of our model. Fig. 5 shows that for both choices the Holstein model exhibits a much weaker response to the pump than does the quadratic model, exhibiting both a much weaker enhancement of double occupancy (uppermost panel), and smaller large-amplitude dynamics in momentum-resolved electronic correlations (lower panels) including flattening of $P_k(t)$ (lowermost panel). We remark that the dynamics governed by the quadratic model exhibits very weak behavior in the zero-pump limit $\alpha = 0$ (not shown), highlighting the susceptibility of the non-linear coupling to photo-excited vibrations.

V. CONCLUSIONS

Prior studies of non-linear electron-phonon dynamics have relied on approximate low-energy treatments when no small parameter exists. Our exact numerical approach to spatially resolved dynamics of a pumped non-linear

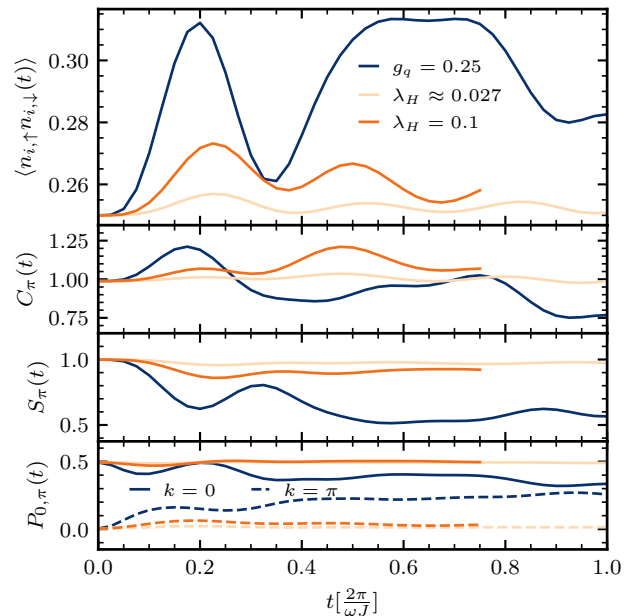


FIG. 5. **Quadratically coupled model versus Holstein model.** A comparison of the pump-induced dynamics in the quadratic coupling model to that of the Holstein model for appropriately selected couplings and $\omega = \pi/2$ (see text and Appendix E for more details) reveals that the driven quadratic model induces a more appreciably enhanced double occupancy (uppermost panel) and causes a greater response in electron correlations (lower three panels) including the flattening of pairing tendencies (lowermost panel) than its Holstein model counterpart.

electron-phonon systems fills an urgent need. We provide a detailed exact analysis of short-time (up to $t \sim \frac{2\pi}{\omega J}$) dynamics of an infinite non-linear electron-phonon coupled metal upon coherent excitation of vibrational modes by light using iTEBD. We supplement this by direct Krylov propagation of small systems to asymptotically long times. We explicitly describe the flow towards a correlated electron-phonon steady state at long times, the indication of which already manifests on short timescales. Remarkably, although we consider a spatially uniform system evolving after application of a spatially uniform pump field, the key feature of the long-time state is the appearance of properties consistent with a high degree of effective disorder that dominates the physical properties. These properties are a consequence of the very rapid loss of coherence of the initial phonon state created by the pump, which we found to be directly tied to the buildup of disorder, implying that the intermediate- and long-time state is an incoherent superposition of different oscillator configurations on different sites. These incoherent phonon configurations result in a dynamic effective disorder potential for the electrons, which leads to the suppression of long-range charge, spin and pairing correlations.

The single-particle distribution function of the long-

time electronic state found in finite-size systems for $\alpha = \sqrt{2}$ may be fit to a Fermi-Dirac distribution with a temperature $T_e \sim 2J$ (we could not find a good fit for long-time states obtained for small α values). On the other hand, the corresponding Poisson-like phonon state exhibits a maximum in occupation numbers ν and therefore does not fit a thermal Planck distribution. Of course, in a strongly coupled electron-phonon system a Planck distribution is not expected. However, the high-energy tail should still decay in a manner controlled by the equilibrium temperature. A fit of the exponentially decaying phonon occupation tail to the Planck distribution yields a pseudo-temperature $T_{\text{ph}} \sim 5J$. This mismatch between T_e and T_{ph} along with the large contribution of the electron-phonon interaction term to the total energy suggests that the terminal state obtained in finite-size simulations may not be thermal. Determining the fate of the established long-time entangled electron-phonon state in which the phonons in effect provide strong onsite potential fluctuations that substantially broaden all momentum-space distribution functions and fully disentangling the contributions of electron heating from localization due to the transient phonon-induced disorder to this entangled electron-phonon state are beyond the scope of this paper, and are left to future work.

A crucial question, not resolved by this work, relates to the possibility of pump-induced superconductivity as predicted in Ref. [13]. In our calculations no evidence for superconductivity is found and we only find weak evidence for charge density wave correlations: the results are more consistent with the system falling within the disorder-dominated Anderson insulating regime of the phase diagram presented in Ref. [13]. One possibility would be that superconducting and density wave regimes either do not exist or are not accessible with the current pump protocol (perhaps because the pump transfers too much energy to the electronic subsystem). A second possibility would be that the one-dimensional model considered here disfavors superconductivity. In fact, it has been shown that quantum fluctuations can destroy superconductivity in dirty superconductors below a mobility threshold [31]. In one dimension, all single-particle states are localized in presence of a static disorder potential. Despite that in one-dimensional systems superconductivity can overcome the localizing tendency of disorder to some extent [32], the effects of disorder are stronger than in higher dimensions. The accurate simulation of pump-induced dynamics in higher-dimensional systems in the thermodynamic limit faces challenges, but is urgently needed.

Lastly, we noted that the quadratic model reacts more strongly to a pump than the linear Holstein model, highlighting the importance of this mechanism in pump-probe experiments, e.g. [33]. Our results generally apply to light irradiated centrosymmetric crystals. Questions such as the consideration of additional electron-vibration interactions consistent with inversion symmetry [20, 34], which may aid in the stabilization of a transient superconducting state, as well as how the the electron-phonon steady

state exposed in this work manifests experimentally are also important open challenges and call for the development of new tools for the study of out-of-equilibrium non-linear electron-phonon problems.

ACKNOWLEDGMENTS

J. S. acknowledges the hospitality of the Center for Computational Quantum Physics (CCQ) at the Flatiron Institute. J. S., D. R. R. and A. J. M. acknowledge support from the National Science Foundation (NSF) Materials Research Science and Engineering Centers (MRSEC) program through Columbia University in the Center for Precision Assembly of Superstratic and Superatomic Solids under Grant No. DMR-1420634. B. K. acknowledges support from NSF Grant No. CHE-1954791. D. M. K. acknowledges support from Deutsche Forschungsgemeinschaft (DFG, German Research Foundation) under Germany's Excellence Strategy - Cluster of Excellence Matter and Light for Quantum Computing (ML4Q) EXC 2004/1 - 390534769 and from the Max Planck-New York City Center for Non-Equilibrium Quantum Phenomena. This work used the Extreme Science and Engineering Discovery Environment (XSEDE), which is supported by NSF grant number ACI-1548562, through allocation TG-DMR190074.

Appendix A: Stability condition of the quadratic electron-phonon model

The model we consider reads

$$\mathcal{H} = \mathcal{H}_e + \mathcal{H}_{\text{ph}} + \mathcal{V}_{\text{e-ph}}, \quad (\text{A1})$$

where

$$\mathcal{H}_e = -J \sum_{i,\sigma} c_{i,\sigma}^\dagger c_{i+1,\sigma} + \text{H.c.}, \quad (\text{A2})$$

$$\mathcal{H}_{\text{ph}} = \omega \sum_i \left(b_i^\dagger b_i + \frac{1}{2} \right), \quad (\text{A3})$$

$$\mathcal{V}_{\text{e-ph}} = g_q \sum_i (\hat{n}_i - 1) (b_i^\dagger + b_i)^2. \quad (\text{A4})$$

A stable harmonic oscillator mode localized on a given site implies an oscillator stiffness $K > 0$. To derive the condition for stability of the coupled electron-phonon system, we rewrite \mathcal{H} in terms of the harmonic oscillator displacement \hat{X}_i and momentum \hat{P}_i operators. We make use of the relation ($\hbar = 1$)

$$b_i = \sqrt{\frac{M\omega}{2}} \left(\hat{X}_i + \frac{1}{m\omega} \hat{P}_i \right), \quad (\text{A5})$$

where M is the oscillator mass, to obtain

$$\mathcal{H}_{\text{ph}} = \sum_i \frac{1}{2} K \hat{X}_i^2 + \sum_i \frac{1}{2M} \hat{P}_i^2 \quad (\text{A6})$$

$$\mathcal{V}_{\text{e-ph}} = 2 \frac{g_q}{\omega} K \sum_i (\hat{n}_i - 1) \hat{X}_i^2. \quad (\text{A7})$$

Thus, the quadratic electron-phonon coupling renormalizes the oscillator stiffness on any given site

$$K \rightarrow K \left[1 + 4(\hat{n} - 1) \frac{g_q}{\omega} \right]. \quad (\text{A8})$$

Demanding that $K > 0$, we arrive at the stability condition of the electron-phonon model:

$$|g_q| < \frac{\omega}{4}. \quad (\text{A9})$$

For spinless electrons $\hat{n} - 1 \rightarrow \hat{n} - 1/2$ and the stability condition, then, is $|g_q| < \frac{\omega}{2}$.

Appendix B: Squeezing transformation

Kennes et al. [13] found a transformation that rescales the phonon coordinate, rotating the Hamiltonian Eq. (A1) into a frame in which the electrons and phonons are approximately decoupled. The electron density-dependent transformation $\mathcal{H} \rightarrow U\mathcal{H}U^\dagger$, with $U = e^S$, $S = -\sum_j \zeta_j (b_j^\dagger b_j^\dagger - b_j b_j)$ and squeezing parameter $\zeta_i = -\frac{1}{4} \ln[1 + 4\frac{g_q}{\omega}(\hat{n}_i - 1)]$, yields

$$\begin{aligned} \beta_i^\dagger &\equiv e^S b_i^\dagger e^{-S} = \cosh(\zeta_i) b_i^\dagger + \sinh(\zeta_i) b_i, \\ \beta_i &\equiv e^S b_i e^{-S} = \cosh(\zeta_i) b_i + \sinh(\zeta_i) b_i^\dagger. \end{aligned} \quad (\text{B1})$$

Here β_i^\dagger creates a squeezed phonon state on site i . Under this transformation, $\mathcal{H}_{\text{ph}} + \mathcal{V}_{\text{e-ph}}$ is recast into a form completely diagonal in the squeezed phonon occupation basis:

$$\mathcal{H} = e^S \mathcal{H}_e e^{-S} + \sum_i \omega \sqrt{1 + 4\frac{g_q}{\omega}(\hat{n}_i - 1)} (\beta_i^\dagger \beta_i + \frac{1}{2}). \quad (\text{B2})$$

Taylor expanding to $\mathcal{O}\left\{\left(\frac{g_q}{\omega}\right)^2\right\}$, one finds

$$\begin{aligned} \mathcal{H} &= e^S \mathcal{H}_e e^{-S} + \sum_i \omega (\beta_i^\dagger \beta_i + \frac{1}{2}) \\ &+ \sum_i \left[2(g_q + \frac{g_q^2}{\omega}) (\beta_i^\dagger \beta_i + \frac{1}{2}) \right] (\hat{n}_i - 1) \\ &+ \sum_i -4\frac{g_q^2}{\omega} (\beta_i^\dagger \beta_i + \frac{1}{2}) \hat{n}_{i,\uparrow} \hat{n}_{i,\downarrow}. \end{aligned} \quad (\text{B3})$$

To this order the electron-phonon coupling is completely local and the squeezed phonon number on each site is conserved. The second line shows that the phonon occupation on site i changes the electron's local chemical potential. This gives rise to a disorder potential, static at this level of approximation. Higher-order terms neglected in the transformation will lead to the evolution of $\beta_i^\dagger \beta_i$, changing the disorder from static to dynamic. Phonons also mediate an effective local electron-electron attraction (third line). The $e^S \mathcal{H}_e e^{-S}$ term can be treated analytically within an incoherent approximation, see [13] for details.

Appendix C: Details of iTEBD simulations

The quadratic electron-phonon model connects a phonon state of occupancy ν only to states with $\nu' = \nu \pm 2$. These processes conserve phonon parity. We take advantage of this symmetry and parallelize most simulations over even and odd phonon parity subsectors employing up to $d_\nu = 12$ states, see discussion below. We use a fourth-order trotterization scheme for the iTEBD time evolution with time-steps dt . After each time-step, we truncate the Schmidt values of a two-site unit cell state embedded in an infinite system; the discarded Schmidt values squared ϵ_{TEBD} denotes the error due to truncation. We ensure that the bond dimension χ of the time-evolved state after each time-step does not saturate an upper bound we set, which we take to be, for the data points we study, in the range of 3000 – 5000. We converge our results with respect to both dt and ϵ_{TEBD} , as we explain below.

1. Convergence with respect to dt and ϵ_{TEBD}

Errors due to dt compete with those due to ϵ_{TEBD} . A sufficiently small dt ensures negligible Trotter error. At the same time, however, it results in more frequent incidents of truncation of the Schmidt values, each of an amount $\sqrt{\epsilon_{\text{TEBD}}}$, thus leading to overall greater Schmidt truncation in order to access a specific desired final time t_f . A sufficiently small ϵ_{TEBD} would eliminate Schmidt errors to within a desirable accuracy, but instead leads to faster growth of entanglement, which scales exponentially in time, and this limits the accessible t_f . To ensure accurate results one needs to converge results with respect to the competing effects due to dt and ϵ_{TEBD} , finding an optimal compromise of a sufficiently small (but not too small) dt to eliminate Trotter error given a reasonably small ϵ_{TEBD} to ensure minimal error due to Schmidt truncation. In Fig. 6, we demonstrate convergence for two quantities $P_k(t)$ and $C_k(t)$. The same choices of dt and ϵ_{TEBD} allows convergence of all other quantities considered in this work to the same standard or better. This allows us to approach $t_f \sim 5J^{-1}$.

2. Convergence with respect to d_ν

We converge results for electronic and phononic observables with respect to the phonon Hilbert space dimension d_ν within a reasonable accuracy of a few percent. Fig. 7 shows satisfactory convergence of representative quantities for $d_\nu = 12$, which we use to obtain the data presented in the main text.

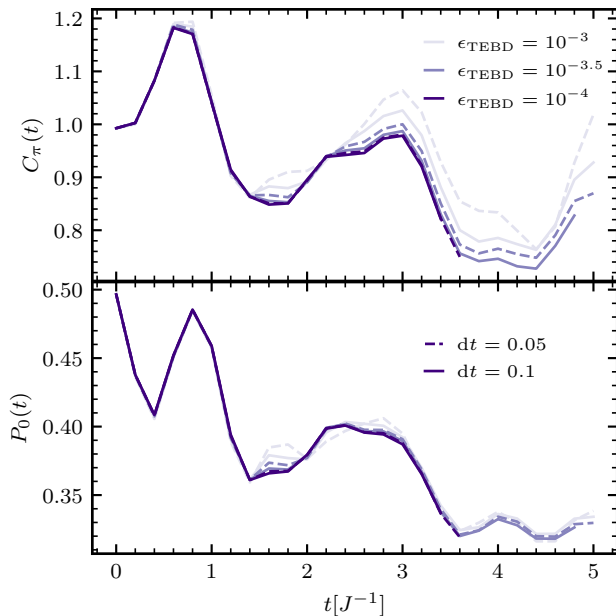


FIG. 6. Convergence of time-evolved charge $C_k(t)$ and pairing $P_k(t)$ correlations with respect to truncation error ϵ_{TEBD} and time-step dt used in iTEBD simulations. We use $g_q = 0.25$ and $\omega = \pi/2$ here, which enables the assessment of convergence for the strongest coupling considered. We observe satisfactory convergence for $\epsilon_{\text{TEBD}} = 10^{-3.5}$ and $dt = 0.1$ on the accessible timescales.

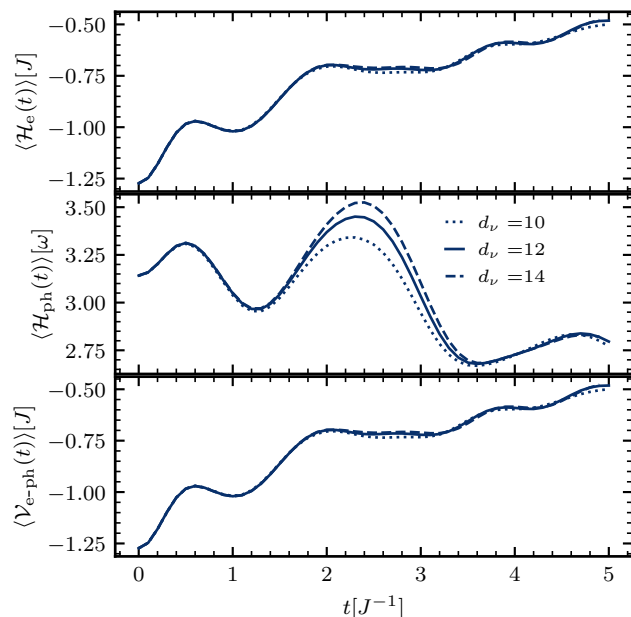


FIG. 7. Convergence of time-evolved energy densities $\langle \mathcal{H}_e(t) \rangle$, $\langle \mathcal{H}_{\text{ph}}(t) \rangle$ and $\langle \mathcal{V}_{\text{e-ph}}(t) \rangle$ with respect to local phonon Hilbert space dimension d_ν used in iTEBD simulations. We use $\epsilon_{\text{TEBD}} = 10^{-3.5}$ in the simulation performed here for $g_q = 0.25$ and $\omega = \pi/2$. We find that $d_\nu = 12$ suffices to achieve convergence within a reasonable bound at all accessible times.

Appendix D: Details of propagation using direct Krylov subspace methods

We perform exact time evolution via direct Krylov space methods for system sizes $L = 3 - 6$, employing parallelization with respect to the local bosonic parity sectors. We use a twisted boundary condition: $e^{i(\pi/2)L}$ in the simulations presented in the main text. For small system sizes, convergence with respect to the local bosonic Hilbert space dimension can be achieved, while for $L = 6$ we are restricted to a truncated bosonic Hilbert space dimension $d_\nu = 10$.

Appendix E: Choice of Holstein couplings used to compare to a quadratic coupling

The Holstein model with electron-phonon coupling $g_H(\hat{n}_i - 1)(b_i^\dagger + b_i)$ can be characterized via the dimensionless coupling $\lambda_H = \frac{g_H^2}{2\omega J}$, the ratio of the ground-state energy in the atomic limit $J = 0$ to that in the free electron limit $g_H = 0$. To compare the Holstein and quadratic models one must find the λ_H most comparable to a given quadratic coupling. We consider the two following approaches to estimate measures of equivalence of coupling strengths:

a. *Coupling strengths that give the same double occupancy in the static equilibrium limit:*

We find for $\omega = \pi/2$, $g_q = 0.25$ and $g_H = 0.29$ ($\lambda_H \approx 0.027$) yield the same double occupancy in the ground state of a half-filled chain.

b. *Coupling strengths that give the same effective electron-electron interaction obtained from a disentangling transformation:*

The Lang-Firsov transformation [35] demonstrates that Holstein phonons mediate an effective electron-electron attraction $U_H = -2\frac{g_H^2}{\omega} \equiv -4\lambda_H J$. The squeezing transformation derived above demonstrates that quadratic phonons mediate an effective electron-electron attraction $U_q = -4\frac{g_q^2}{\omega} \left(\langle n_{B,i} \rangle + 1/2 \right)$, where $n_{B,i} = \beta_i^\dagger \beta_i$, see Eq. (B3). The two models yield the same U when $U_H = U_q$, leading to the condition:

$$\lambda_H = \frac{g_q^2}{\omega J} \left(\langle n_B \rangle + 1/2 \right), \quad (\text{E1})$$

where we replaced the phonon number operator by its average over the phonon distribution $\langle n_B \rangle$. Since the radiation field creates a coherent state with amplitude α , we take an estimate of $\langle n_B \rangle = \alpha^2$ the mean boson number to find λ_H to be used to compare against a given g_q . We thus judge for $\alpha = \sqrt{2}$ and $\omega = \pi/2$ $\lambda_H \approx 0.1$ to be equivalent to $g_q = 0.25$ in the sense that it leads to an effective electron-electron interaction approximately equal to that obtained from the *pumped* quadratic model (as analyzed within the squeezing transformation).

To summarize, we employ two methods to estimate a value of λ_H to compare to a given value of g_q . One approach assumes the two models are comparable when they yield the same double occupancy in the static ground-state limit, the other compares the undriven Hol-

stein model to the driven quadratic model, making use of analytical results. We can conceptually use these two values of λ_H as approximate lower and upper bounds for comparison against a given value of g_q .

-
- [1] D. N. Basov, R. D. Averitt, D. van der Marel, M. Dressel, and K. Haule, “Electrodynamics of correlated electron materials,” *Rev. Mod. Phys.* **83**, 471 (2011).
- [2] C. Giannetti, M. Capone, D. Fausti, M. Fabrizio, F. Parmigiani, and D. Mihailovic, “Ultrafast optical spectroscopy of strongly correlated materials and high-temperature superconductors: A non-equilibrium approach,” *Adv. Phys.* **65**, 58 (2016).
- [3] S. Wall, D. Prabhakaran, A. T. Boothroyd, and A. Cavalleri, “Ultrafast coupling between light, coherent lattice vibrations, and the magnetic structure of semicovalent LaMnO_3 ,” *Phys. Rev. Lett.* **103**, 097402 (2009).
- [4] G. A. Garrett, A. G. Rojo, A. K. Sood, J. F. Whitaker, and R. Merlin, “Vacuum squeezing of solids: Macroscopic quantum states driven by light pulses,” *Science* **275**, 1638 (1997).
- [5] M. Rini, R. Tobey, N. Dean, J. Itatani, Y. Tomioka, Y. Tokura, R. W. Schoenlein, and A. Cavalleri, “Control of the electronic phase of a manganite by mode-selective vibrational excitation,” *Nature* **449**, 72 (2007).
- [6] B. He, C. Zhang, W. Zhu, Y. Li, S. Liu, X. Zhu, X. Wu, X. Wang, H.-h. Wen, and M. Xiao, “Coherent optical phonon oscillation and possible electronic softening in WTe_2 crystals,” *Sci. Rep.* **6**, 30487 (2016).
- [7] M. Mitranò, A. Cantaluppi, D. Nicoletti, S. Kaiser, A. Perucchi, S. Lupi, P. Di Pietro, D. Pontiroli, M. Riccò, S. R. Clark, D. Jaksch, and A. Cavalleri, “Possible light-induced superconductivity in K_3C_{60} at high temperature,” *Nature* **530**, 461 (2016).
- [8] B. Liu, M. Först, M. Fechner, D. Nicoletti, J. Porras, T. Loew, B. Keimer, and A. Cavalleri, “Pump frequency resonances for light-induced incipient superconductivity in $\text{YBa}_2\text{Cu}_3\text{O}_{6.5}$,” *Phys. Rev. X* **10**, 011053 (2020).
- [9] M. Buzzi, D. Nicoletti, M. Fechner, N. Tancogne-Dejean, M. A. Sentef, A. Georges, T. Biesner, E. Yukur, M. Dressel, A. Henderson, T. Siegrist, J. A. Schlueter, K. Miyagawa, K. Kanoda, M.-S. Nam, A. Ardavan, J. Coulthard, J. Tindall, F. Schlawin, D. Jaksch, and A. Cavalleri, “Photomolecular high-temperature superconductivity,” *Phys. Rev. X* **10**, 031028 (2020).
- [10] M. Först, C. Manzoni, S. Kaiser, Y. Tomioka, Y. Tokura, R. Merlin, and A. Cavalleri, “Nonlinear phononics as an ultrafast route to lattice control,” *Nat. Phys.* **7**, 854 (2011).
- [11] A. Subedi, A. Cavalleri, and A. Georges, “Theory of nonlinear phononics for coherent light control of solids,” *Phys. Rev. B* **89**, 220301 (2014).
- [12] R. Mankowsky, M. Först, and A. Cavalleri, “Nonequilibrium control of complex solids by nonlinear phononics,” *Rep. Prog. Phys.* **79**, 064503 (2016).
- [13] D. M. Kennes, E. Y. Wilner, D. R. Reichman, and A. J. Millis, “Transient superconductivity from electronic squeezing of optically pumped phonons,” *Nat. Phys.* **13**, 479 (2017).
- [14] M. A. Sentef, A. F. Kemper, A. Georges, and C. Kollath, “Theory of light-enhanced phonon-mediated superconductivity,” *Phys. Rev. B* **93**, 144506 (2016).
- [15] M. Kim, Y. Nomura, M. Ferrero, P. Seth, O. Parcollet, and A. Georges, “Enhancing superconductivity in A_3C_{60} fullerenes,” *Phys. Rev. B* **94**, 155152 (2016).
- [16] M. Knap, M. Babadi, G. Refael, I. Martin, and E. Demler, “Dynamical Cooper pairing in nonequilibrium electron-phonon systems,” *Phys. Rev. B* **94**, 214504 (2016).
- [17] M. A. Sentef, “Light-enhanced electron-phonon coupling from nonlinear electron-phonon coupling,” *Phys. Rev. B* **95**, 205111 (2017).
- [18] M. Babadi, M. Knap, I. Martin, G. Refael, and E. Demler, “Theory of parametrically amplified electron-phonon superconductivity,” *Phys. Rev. B* **96**, 014512 (2017).
- [19] Y. Murakami, N. Tsuji, M. Eckstein, and P. Werner, “Nonequilibrium steady states and transient dynamics of conventional superconductors under phonon driving,” *Phys. Rev. B* **96**, 045125 (2017).
- [20] F. Grandi, J. Li, and M. Eckstein, “Ultrafast Mott transition driven by nonlinear phonons,” *arXiv:2005.14100* (2020).
- [21] T. Holstein, “Polaron motion. I. Molecular-crystal models,” *Ann. Phys.* **8**, 325 (1959).
- [22] H. Fröhlich, H. Pelzer, and S. Zienau, “Properties of slow electrons in polar materials,” *Philos. Mag.* **41**, 221 (1950).
- [23] H. Fröhlich, “Electrons in lattice fields,” *Adv. Phys.* **3**, 325 (1954).
- [24] R. J. Glauber, “Coherent and incoherent states of the radiation field,” *Phys. Rev.* **131**, 2766 (1963).
- [25] N. W. Ashcroft and N. D. Mermin, *Solid state physics* (Holt, Rinehart and Winston, New York, 1976).
- [26] P. Calabrese and J. Cardy, “Time dependence of correlation functions following a quantum quench,” *Phys. Rev. Lett.* **96**, 136801 (2006).
- [27] This coupling also serves as a description of double-well electron-phonon systems [36, 37].
- [28] G. Vidal, “Classical simulation of infinite-size quantum lattice systems in one spatial dimension,” *Phys. Rev. Lett.* **98**, 070201 (2007).
- [29] J. Hauschild and F. Pollmann, “Efficient numerical simulations with Tensor Networks: Tensor Network Python (TeNPy),” *SciPost Phys. Lect. Notes*, 5 (2018).
- [30] M. H. Kalthoff, D. M. Kennes, and M. A. Sentef, “Floquet-engineered light-cone spreading of correlations in a driven quantum chain,” *Phys. Rev. B* **100**, 165125 (2019).
- [31] M. Ma, B. I. Halperin, and P. A. Lee, “Strongly disordered superfluids: Quantum fluctuations and critical behavior,” *Phys. Rev. B* **34**, 3136 (1986).
- [32] T. Giamarchi and H. J. Schulz, “Anderson localization and interactions in one-dimensional metals,” *Phys. Rev.*

- B **37**, 325 (1988).
- [33] C. Hwang, W. Zhang, K. Kurashima, R. Kaindl, T. Adachi, Y. Koike, and A. Lanzara, “Ultrafast dynamics of electron-phonon coupling in a metal,” *Europhys. Lett.* **126**, 57001 (2019).
- [34] J. Sous, M. Chakraborty, R. V. Krems, and M. Berciu, “Light bipolarons stabilized by Peierls electron-phonon coupling,” *Phys. Rev. Lett.* **121**, 247001 (2018).
- [35] I. Lang and Y. A. Firsov, “Kinetic theory of semiconductors with low mobility,” *Soviet J. Exp. Theor. Phys.* **16**, 1301 (1963).
- [36] C. P. J. Adolphs and M. Berciu, “Single-polaron properties for double-well electron-phonon coupling,” *Phys. Rev. B* **89**, 035122 (2014).
- [37] C. P. J. Adolphs and M. Berciu, “Strongly bound yet light bipolarons for double-well electron-phonon coupling,” *Phys. Rev. B* **90**, 085149 (2014).